Characterization of diamond adhesion on micro-grain WC–Co substrates using Brinell indentations and micro-Raman spectroscopy

2004 J. Phys.: Condens. Matter 16 6661

(http://iopscience.iop.org/0953-8984/16/37/003)

INSTITUTE OF PHYSICS PUBLISHING JOURNAL OF PHYSICS: CONDENSED MATTER

J. Phys.: Condens. Matter **16** (2004) 6661–6674 PII: S0953-8984(04)82818-2

Characterization of diamond adhesion on micro-grain WC–Co substrates using Brinell indentations and micro-Raman spectroscopy

N Ali[1], G Cabral[1], E Titus[1], A A Ogwu[2] and J Gracio[1]

[1] Centre for Mechanical Technology and Automation, University of Aveiro, 3810-193 Aveiro, Portugal
[2] Thin Film Centre, University of Paisley, PA1 2BE, UK

E-mail: n.ali@mec.ua.pt

Received 29 June 2004, in final form 12 August 2004
Published 3 September 2004
Online at stacks.iop.org/JPhysCM/16/6661
doi:10.1088/0953-8984/16/37/003

Abstract

In this study, we investigate the adhesion of diamond coatings deposited on 0.8 μm WC–10% Co substrates using chemical vapour deposition (CVD). Polycrystalline diamond films were deposited using (i) constant methane (CH_4) flow, at 3 and 4.5 sccm, and (ii) modulated CH_4 flow at 4.5 and 3 sccm for 8 and 10 min, respectively. Constant CH_4 flow into the vacuum chamber during diamond CVD is the conventional approach to deposit diamond onto a range of substrate materials. The timed CH_4 modulations are an integral part of our recently proposed process called time-modulated CVD (TMCVD). The coating adhesion was characterized using indentation tests employing a Brinell indenter. In this study, we employ three indentation loads: 294, 490 and 612.5 N. In addition, micro-Raman spectroscopy was used to (i) characterize the deposited films for diamond-carbon phase purity and (ii) determine the biaxial stresses in the coating samples. In this paper, we correlate the adhesion strength of diamond films to biaxial stresses.

No lateral cracking occurred in diamond films deposited by the TMCVD process after a 294 N load indentation. This result coupled with the complementary stress calculations indicates a higher film–substrate adhesion in time-modulated films. Our findings suggest that at higher indentation loads the response from and the behaviour of the substrate need to be considered in determining the coating adhesion strength. The TMCVD process promotes secondary nano-sized diamond crystallites during the higher timed methane modulations. It is expected that the mechanical interlock at the film/substrate interface is higher for film coatings deposited using TMCVD, thus resulting in the improved adhesion of the time-modulated coating on WC–Co.

1. Introduction

Diamond coatings find use in a wide range of industrial applications mainly due to their exceptional and outstanding combination of properties [1–4]. The majority of the applications of diamond coatings demand sufficiently adherent coatings onto a number of materials. Diamond can be deposited onto a variety of materials and the substrates can be classified into the following three main groups.

- Strong carbide forming materials, including Si, Ti, Cr, W, SiC, WC etc.
- Strong carbon dissolving materials, including Fe, Co, Ni etc.
- Small or non-carbon-affinity materials, such as Cu and Au.

Diamond deposition onto carbide forming materials, such as those mentioned above, usually produce reasonably adherent coatings. On the other hand, diamond grown directly onto strong carbon dissolving materials, such as steel or cemented WC–Co or on non-carbon-affinity materials, such as copper, yields poor adhesion [5–10].

Cemented WC–Co hard metals containing WC grains in the sub-micron (0.5–0.8 μm) to ultra-fine (0.2–0.5 μm) range and also containing 6–16 wt% of cobalt (Co) generally find use in micro-machining applications, dental burs, surgical tools, microdrills, punches used in the pharmaceutical industry, etc [11]. Although such grades of hard metals display impressive properties, such as toughness, their performance during service and lifetime is not ideal for many of the applications. However, improvements in such areas can be achieved by the application of a diamond coating onto the component. Generally, the task of direct diamond deposition onto WC–Co hard metals is notoriously difficult. In particular, deposition onto grades of cemented WC–Co, consisting of sub-micron or ultra-fine grains of WC and/or high content of Co (>8 wt%), becomes an even more difficult endeavour. Generally, as the WC-grain size increases and/or the Co content (%) in the hard metal decreases, diamond CVD onto WC–Co becomes less problematic. Since diamond deposition onto cemented WC–Co consisting of finer sized WC grains and high percentage content of Co is difficult, less work has been performed on these grades of hard metals [12–15]. However, many papers can be found in the open literature reporting diamond deposition onto coarse grain WC–Co hard metals with Co contents even less than 8% [16–27]. The major cause of concern that prevents the successful deposition of diamond onto WC–Co is the negative effects of Co on film growth [28]. However, a number of surface pre-treatment methods have been used to minimize the problems relating to the presence of Co in the cemented-WC substrate during diamond CVD. Generally, the surface pre-treatment methods employed can be classed into three groups: namely, (i) chemical treatments [29]; (ii) stable cobalt compounds [30]; and (iii) intermediate metallic/ceramic layers [31].

CVD continues to be a very powerful technique for depositing diamond films onto a range of materials and components [32]. Generally, diamond deposition in a CVD reactor is traditionally performed under constant flow of CH_4 in excess hydrogen. Recently, we proposed the TMCVD process, which facilitates the growth of improved micro- and nano-crystalline diamond coatings onto silicon wafers by using timed CH_4 modulations [33]. Furthermore, the process gives greater control over film microstructure by adjusting the key process parameters during film growth. In this paper, we implement the TMCVD process and thus employ timed CH_4 modulations to improve the coating adhesion of diamond films deposited onto 0.8 μm WC–10% Co substrates. It is known that the poor adhesion of film coatings on cutting tools can lead to catastrophic failure of the coating in metal cutting operations [34]. Therefore, improving the coating adhesion becomes both needful and timely.

Table 1. Conditions employed during the preparation of the samples 1–3.

	Samples		
Parameter	1	2	3
Filament to substrate distance (mm)	4	4	4
Deposition pressure (Pa)	4000	4000	4000
CH_4 flow (sccm)	3	4.4	4.5, 3
CH_4 modulation time (min)	—	—	10, 8
Hydrogen flow (sccm)	150	150	150
Substrate temperature (°C)	850	850	850
Deposition time (min)	126	126	126

Over the years, a number of adhesion test methods have been used to characterize the diamond coating adhesion. These methods include pull-off, scratch and indentation tests [35]. The pull-off tests are accurate and quantitative if only the pulling force can be calibrated well normal to the sample surface. The main difficulty encountered with this type of method is that the tested critical force is limited by the strength of the adhesive, normally weaker than 90 MPa. Thus, the adhesive usually fails prior to the diamond coatings [35]. Adhesion scratch tests are widely used to characterize the coating adhesion. However, the high hardness of the polycrystalline diamond coating leads to a cleavage of the scratch tip even after a single pass, which has obvious consequences in both economics and repeatability. As a comparison, the indentation tests reduce considerably the possible damage to the indenter tip and therefore are more practically suited for characterizing the coating adhesion.

The present work focuses on using indentation tests employing a Brinell indenter to characterize the coating adhesion. Further, residual stresses which play a critical role in governing the diamond coating adhesion have been characterized using micro-Raman spectroscopy. The shifting and the splitting of the Raman peaks have been related to the adhesion strength at the coating/substrate interface. Raman spectroscopy has the advantage of being a non-destructive technique, which could be interesting for use in quality control.

2. Experimental details

The WC–Co hard metal substrates (10 mm × 10 mm × 3 mm) contained 10% cobalt and the WC grain size was 0.8 μm. After being freshly cut to size, the substrates were ground using a diamond wheel and subsequently polished using 3 μm diamond paste for a time duration until the average substrate surface roughness was in the range $0.9 < R_a < 1.1$. After the polishing pre-treatments, the substrates were ultrasonically cleaned in acetone for 10 min in order to remove any loose residues. The substrates were then chemically etched in Murakami solution (10 g $K_3(Fe(CN)_6)$ + 10 g KOH + 100 ml H_2O), containing diamond powder (0.25 μm in size) for seeding effects, for 15 min in an ultrasonic bath followed by a rinse in distilled water. Subsequently, the substrates were etched for 60 s in HNO_3 (10%) + H_2O_2 (90%) in an ultrasonic bath. Finally, the substrates were ultrasonically cleaned in de-ionized water for 3 min prior to being loaded into the CVD chamber.

The conventional hot filament CVD system which was used to deposit the diamond films has been described elsewhere [36]. Prior to film deposition, the tantalum filament was pre-carburized for 20 min [36]. The filament temperature was approximately 1927 °C. In this study, three diamond coating samples, labelled 1–3, on WC–Co substrates were prepared. Table 1 shows the growth conditions employed during the preparation of samples 1–3. It should be

noted that the flow of CH_4 gas during samples 1 and 2 preparation was kept constant at 3 and 4.5 sccm, respectively. However, in preparing sample 3, the CH_4 flow was modulated at 4.5 sccm/3 sccm for 8 and 10 min, respectively. The deposition time for the three samples was 126 min. The average film thickness of the three samples was $\sim$1 μm. These samples were prepared in order to assess the effectiveness of CH_4 modulations during film growth on the production of improved diamond coatings onto WC–Co substrates, in terms of coating adhesion. Greater details on the CH_4 modulations performed during the TMCVD process can be found in our earlier communication [33]. Each sample was prepared thrice in order to check for repeatability.

The surfaces of the coatings were characterized using scanning electron microscopy (SEM), Hitachi S4100 field emission. The coating adhesion was assessed using an indentation method employing a Brinell indenter. The following indentation loads were employed in this investigation: (i) 294; (ii) 490; and (iii) 612.5 N.

Micro-Raman spectroscopy was used as a complementary technique to assess (i) film quality and (ii) Raman peak shifts and peak splitting. A Renishaw 2000 micro-Raman system with a 633 nm Ar laser was used to characterize the deposited films. It should be noted that the spectrum resolution was 1 cm^{-1}. At this laser wavelength, the non-diamond forms of carbon scatter more effectively than at a shorter excitation wavelength, for example, at 514 nm (Ar ion laser), because of resonance effects [37, 38]. As a result, a longer wavelength laser reveals more non-diamond bands, whereas a shorter wavelength laser usually leads to Raman spectra of lower background and a relatively more intense diamond peak. Therefore, a longer excitation wavelength is useful in characterizing reasonably good quality diamond films, in terms of diamond carbon phase purity. The Raman system works in two modes: (i) main mode and (ii) extended mode. In the main mode the gratings are set at a fixed angle that produces spectra in a narrow range of wavenumbers, for example, 1200–1500 cm^{-1}. However, it gives a high repeatability of ± 0.1 cm^{-1}. On the other hand, the extended mode allows a spectrum range as wide as from -4000 to 4000 cm^{-1}, but the repeatability is usually much poorer compared to the repeatability in the main mode. In order to compare the Raman peak shift, all the spectra in this work were taken in the main mode and a type IIa bulk diamond was used to calibrate the peak position. The Raman system also includes computer software, which can fit the spectra automatically with a Lorentzian function. The diamond peak position is obtained from the best fitting.

3. Results and discussion

3.1. Brinell indentation tests

Figure 1 shows SEM images of samples 1–3 after the 294 N (30 kgf) load indentation. Indentation loads imposed on the diamond coatings in samples 1–3 inflicted noticeable and significant damage only to samples 1 and 2. Each of the SEM image for samples 1 and 2 displayed a structure of the indentation zone that resembled a 'shining sun'. It is evident that some lateral cracking has occurred, in both samples 1 and 2, after the indentations, which corresponds to the 'rays' of the sun on the SEM micrograph images. The average lateral crack lengths in samples 1 and 2 were found to be 102 and 41 μm, respectively. In sample 1, the inner and outer diameters of the deformation zone were found to be 134.69 and 200.87 μm, respectively. A section of the lateral crack on sample 1 was closely examined and a magnified SEM image has also been shown in figure 1. In addition, in sample 1, a lighter region appeared at the circumference of the indentation mark. A magnified SEM image of a specific area in this region, as shown in figure 1, provided evidence that the sample had undergone some film

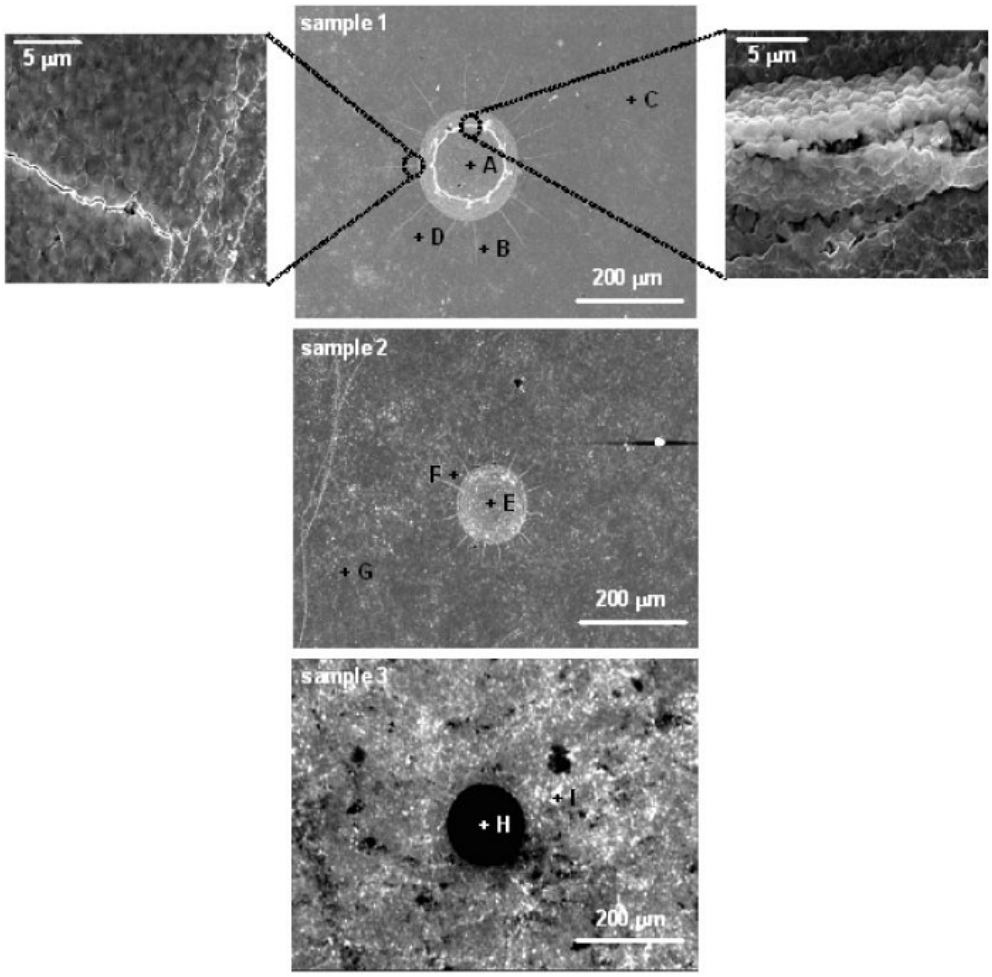

Figure 1. SEM images of samples 1–3 after the 294 N (30 kgf) load indentation.

cracking. However, the cracking of the coating in this region was found to be very localized. It was observed with all three samples that (i) the coatings remained attached to their respective substrates, even after taking into consideration the localized film cracking in sample 1 and the lateral cracking in samples 1 and 2, and (ii) the coating samples deformed to the shape of the Brinell indenter tip. The deformation of the coating samples to the shape of the indenter tip could be expected since plastic deformation in WC–Co substrates occurs during indentation loading.

The lateral cracking in samples 1 and 2 could possibly be due to two factors. First, the external stresses imposed onto the coated-sample during indentation loading could effectively force the film to crack in order to dissipate stress and/or energy. Second, the underlying substrate could fail first and subsequently cause film cracking during plastic deformation at the substrate. In order to monitor the response of the bare (un-coated) 0.8 μm WC–10% Co substrate to the indentation, indentations at the following loads were performed: (i) 294 N; (ii) 490 N; and (iii) 612.5 N. Figure 2 shows the SEM images of the bare, un-coated WC–Co substrate after the indentations at (a) 294 N; (b) 490 N; and (c) 612.5 N loads using the Brinell

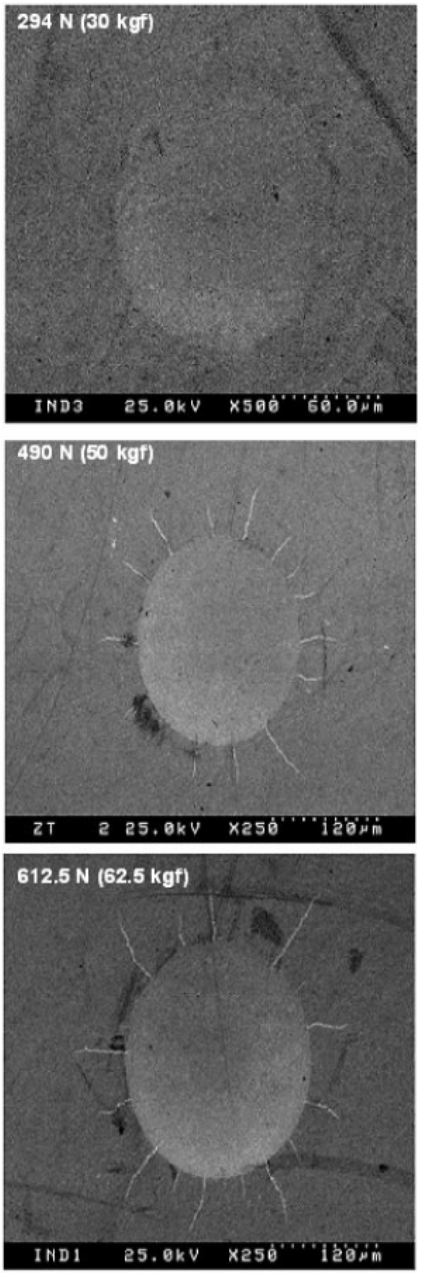

Figure 2. SEM images showing the indented bare, uncoated WC–Co substrates. The indentation loads applied were 294 N (30 kgf), 490 N (50 kgf) and 612.5 N (62.5 kgf).

indenter. It can be seen in figure 2(a) that, although some deformation was observed on the substrate surface, no radial cracks formed at any region on or around the substrate deformation zone. This therefore implies that the lateral cracks appearing in samples 1 and 2 after the 294 N load indentation were due to the limitations of strength at the film/substrate interface. It was found that in sample 3 no radial cracks appeared on the coating surface. The above

indentation tests suggest that the coating adhesion of sample 3 is better than the adhesion toughness in samples 1 and 2. Since, in sample 1, (i) some localized film cracking occurred and (ii) the average radial coating crack length was larger than in sample 2, it can be stated that the coating adhesion of sample 2 is better than in sample 1. It is highly likely that the coating adhesion in sample 3 is better due to the increase in the mechanical interlock between the film and the substrate. Since secondary nucleation processes are predominant in sample 3 preparation [39], using the TMCVD process, and the initial/secondary nucleation rate is much higher, it is expected that the nano-sized diamond crystallites produced strongly interlock with the WC grains of the underlying substrate material.

Indentations at 490 and 612.5 N loads were sufficient to generate apparent radial cracks on the bare substrate materials. The average indentation diameter obtained after the 294, 490 and 612.5 N load indentations were noted to be 122, 183.5 and 209.2 μm, respectively. The grade of the WC–Co substrate material used in this investigation had a fracture toughness value of 13 MN/m^{-3}. The average radial crack length produced at 490 and 612.5 N indentations was measured to be 40.12 and 43.76 μm, respectively. It can be stated that a 490 N (50 kgf) indentation on a bare WC–Co substrate will result in (i) the deformation of the substrate to the shape on the indenter and (ii) the production of radial cracks.

Figure 3 shows SEM micrographs of coating samples 1–3 where a 490 N indentation load was imposed. First, with all three samples 1–3, lateral cracks appeared from the indentations. Second, sample 2 coating delaminated around the deformed zone on the WC–Co substrate. This suggests that the 490 N load indentation was sufficient to debond the film coating from its substrate. Third, in sample 1, SEM analysis showed that the 490 N load indentation had lifted the film coating off from the substrate at points where the apparent radial crack lines ended. However, the film coating remained attached to the substrate from the inner side of the radial cracks. A magnified SEM micrograph, as shown in figure 3, of one region where the radial crack line ended shows the film being lifted off the substrate. In addition, it is also possible to see the lateral crack line appearing on the bare substrate surface. In this region and such other regions in sample 1, the film coating has no contact with the substrate; therefore, no adhesion exists. Fourth, in sample 3, the 490 N indentation load resulted in the following two effects on the indented surface: (i) the formation of lateral cracks and (ii) partial delamination of the film coating in between and across/around some of the lateral cracks. It is possible that in the region on the sample 3 surface where the coating had delaminated from the substrate the mechanical stress imposed by the indenter during indentation loading was too great for the adhesion strength, which kept the coating bonded to the substrate. It is apparent from figure 2(b) that lateral cracks appear on the bare WC–Co material after a 490 N load impression. It could be that the substrate failed first due to the indentation rupture caused by the impression and as a result the strength at the coating/substrate interface had weakened, therefore causing the film to delaminate. In order to assess further the adhesion strength of the coating adhesion in sample 3, another indentation at 612.5 N load was carried out on the sample. Figure 4 shows a SEM micrograph of sample 3, which had been indented at 612.5 N load. The damage inflicted on the sample by the impression is apparent from the SEM image. At this indentation load, the coating adhesion failed. Therefore, it can be stated that the critical load, i.e. the precise load required to delaminate the film coating from the substrate, lies within the range 490–612.5 N.

3.2. Raman spectroscopic analysis

Micro-Raman spectroscopy was employed as a complementary technique to characterize the coating adhesion by assessing the stress levels in the deposited films. It is known that the degree

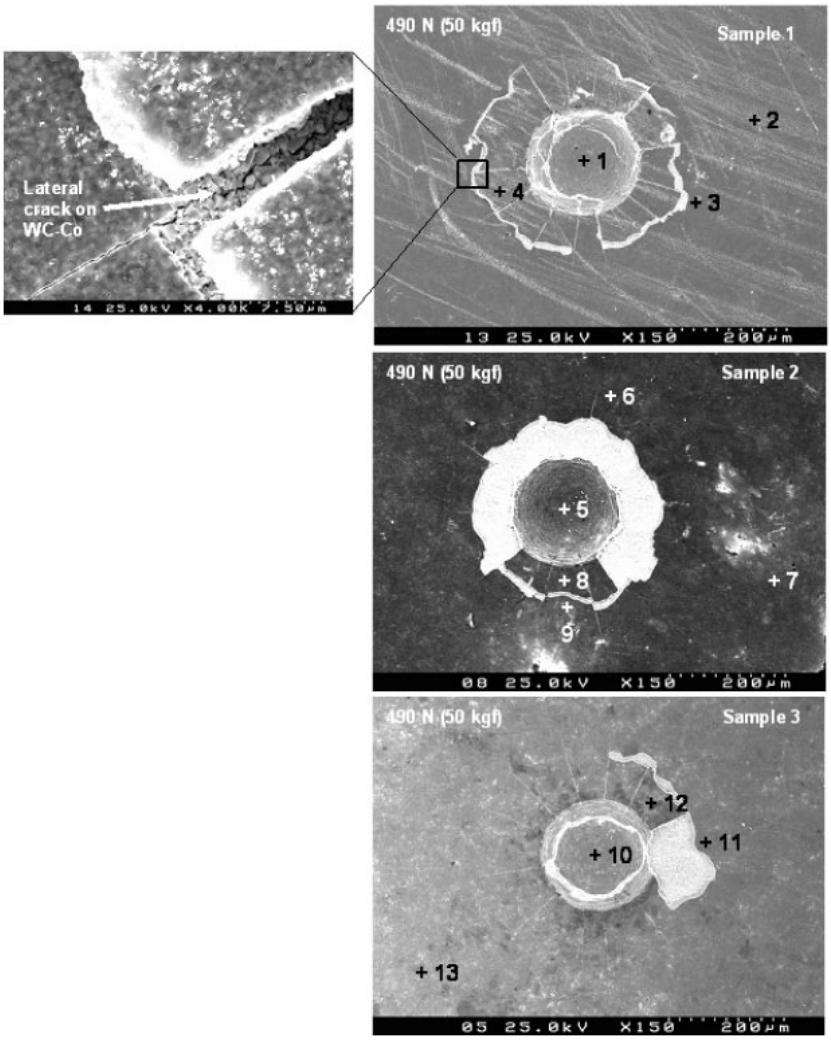

Figure 3. SEM images of the indented samples 1–3 after the application of a 490 N load impression.

of Raman diamond peak shift and the splitting of the peaks is proportional to the magnitude of the biaxial stress in the film [40]. The model developed by Ager and Drory [41], which investigates and characterizes the residual biaxial stresses in diamond films by employing Raman spectroscopy, was used to assess the stress levels in the as-grown films. The model describes quantitatively the relations between singlet or doublet phonon scattering and the biaxial stress σ, measured in GPa, as follows:

$$\sigma = -1.08(\nu_s - \nu_0) \qquad \text{for singlet phonon,} \tag{1}$$

$$\sigma = -0.384(\nu_d - \nu_0) \qquad \text{for doublet phonon,} \tag{2}$$

where $\nu_0 = 1332\ \text{cm}^{-1}$, ν_s is the observed maximum of the singlet in the spectrum and ν_d the maximum of the doublet. In the case when the splitting of the Raman line is not so obvious, the observed peak position ν_m is assumed to be located at the centre between the singlet ν_s and

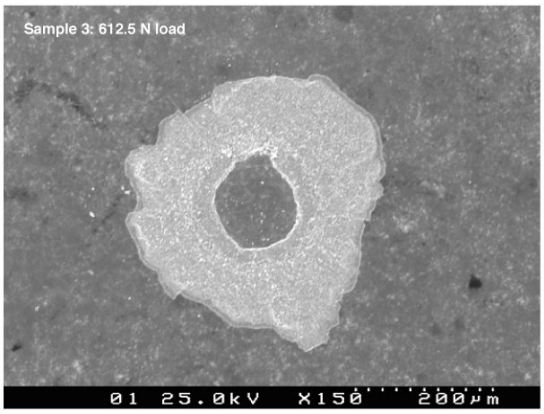

Figure 4. SEM image showing the response of sample 3 to a 612.5 N load indentation.

the doublet ν_d, i.e., $\nu_m = \frac{1}{2}(\nu_s + \nu_d)$ [42]. From equations (1) and (2) we obtain

$$\sigma = -0.567(\nu_m - \nu_0). \tag{3}$$

In this study, equation (3) was used to calculate the film stresses and also determine the nature of the stress, either compressive or tensile.

The points marked A–I and 1–13 on the SEM images in figures 1 and 3 on samples 1–3 will be characterized for stress using micro-Raman spectroscopy. It should be noted that positions A–I are points of characterization on samples that were indented using 294 N (30 kgf) load, whereas points 1–13 (figure 3) appear on coatings that were indented at 490 N (50 kgf) load.

Figure 5 shows the Raman spectroscopy results for characterization points A–D (a), E–G (b) and H–I (c) on samples 1–3, respectively. For sample 1, the Raman diamond peak positions for points A–D were 1333.54, 1335.84, 1339.52 and 1334.84 cm^{-1}, respectively. For sample 2, the Raman peak positions representing points E–G were 1333.54, 1337.22 and 1339.06 cm^{-1}, respectively. Finally, the Raman positions for points H and I on sample 3 were 1334.98 and 1339.98 cm^{-1}, respectively. It is evident from figure 5 that two of the Raman peaks, B and F, underwent line splitting. The splitting on the Raman line in the spectrum signals the presence of increased levels of stress. There was no peak splitting observed in sample 3. Equation (3) was used to calculate the biaxial stress levels in the three coating samples using the Raman peak positions at the different points. Table 2 shows the calculated biaxial stress values for samples 1–3 at positions A–I.

The first point to note is that the minus (−) sign in front of the stress values indicates that the stress is compressive in nature. Compressive stresses are incorporated in films as a result of the differences in the thermal expansion coefficient values between the substrate and the coating material. Second, the Raman spectra for positions C, G and I in samples 1–3, respectively, represents regions of the coatings that are in the as-grown state. It was found that the as-deposited films in samples 1–3 were under compressive stress and the calculated values were −4.26, −4.00 and −4.52 GPa, respectively. The magnitudes of stress in the three samples are almost the same, which can be expected, since the three films were of equal thickness (∼1 μm) and were deposited on the same substrate materials. At positions A, E and H on samples 1–3, the biaxial stresses were calculated to be −0.87, −0.87 and −1.69 GPa, respectively. At these points, the stress in the coatings, is at the minimum level with respect to each coating sample. Therefore, at these points, the coatings are behaving more like stress-free, freestanding diamond films, which display the diamond-characteristic 1332 cm^{-1} peak

Table 2. Biaxial stress values of samples 1–3 at positions A–I. The stress values were obtained using equation (3) and the Raman peak positions.

Sample	Indentation load (N)	Position on sample	Raman peak type	Raman peak position (cm^{-1})	Biaxial stress (−GPa)
	294	A	Singlet	1333.54	0.87
1	(30 kgf)	B	Split	1335.84	2.18
		C	Singlet	1339.52	4.26
		D	Singlet	1334.84	1.61
	294	E	Singlet	1333.54	0.87
2	(30 kgf)	F	Split	1337.22	2.96
		G	Singlet	1339.06	4.00
	294	H	Singlet	1334.98	1.69
3	(30 kgf)	I	Singlet	1339.98	4.52

Table 3. Stress values for samples 1–3 at positions 1–13. The Raman peak positioning at points 1–13 is given together with the type of peak. The stress values were obtained using equation (3).

Sample	Indentation load (N)	Position on sample	Raman peak type	Raman peak position (cm^{-1})	Biaxial stress (−GPa)
		1	Singlet	1333.54	0.87
1	490	2	Singlet	1339.06	4.00
	(50 kgf)	3	Split	1334.92	1.66
		4	Singlet	1334.00	1.13
		5	Singlet	1334.00	1.13
	490	6	Singlet/split	1336.30	2.44
2	(50 kgf)	7	Singlet	1339.52	4.26
		8	Singlet	1334.46	1.39
		9	Split	1338.14	3.48
		10	Singlet	1334.98	1.69
3	490	11	Split	1337.22	2.96
	(50 kgf)	12	Singlet	1334.46	1.39
		13	Singlet	1339.98	4.52

on the Raman spectrum. The imposition of mechanical load on the samples at positions A, E and H weakens the coating adhesion by detaching the films from the substrates and thus releasing some degree of stress from the films at these points. However, it should be noted that at point H (sample 3) the stress is higher with respect to the stress levels at points A and E in samples 1 and 2, respectively. The higher stress value at position H than at points A and E could be held responsible for the increased adhesion strength in sample 3.

The stress in between the radial cracks at positions B, D (sample 1) and F (sample 2) was calculated to be −2.18, −1.61 and −2.96 GPa, respectively, which had significantly reduced compared to the stress in the as-deposited state of the film coatings. This signals the weakening of the adhesion strength in between the radial crack lines.

Figure 6 shows the Raman spectra for coating positions 1–4 (a), 5–9 (b) and 10–13 (c) on samples 1–3, respectively. Table 3 shows the calculated biaxial stress values for positions 1–13 on samples 1–3. As before points 2, 7 and 13 represent the coating samples in the as-deposited state. It is yet again indicative, after the 490 N load indentation, that the biaxial stress at the centre of the indention mark, at point 10, on sample 3 was higher than at points 1 and 5 on samples 1 and 2, respectively. The splitting and partial slitting of the Raman diamond peaks

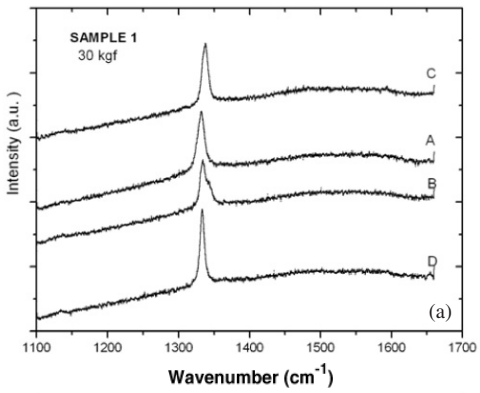

Figure 5. Raman spectra for samples (a) 1, (b) 2 and (c) 3 where each Raman line represents positions A–I (as shown in figure 1). It is important to note that a 294 N indentation load was imposed on the samples, after which the samples were analysed using micro-Raman spectroscopy.

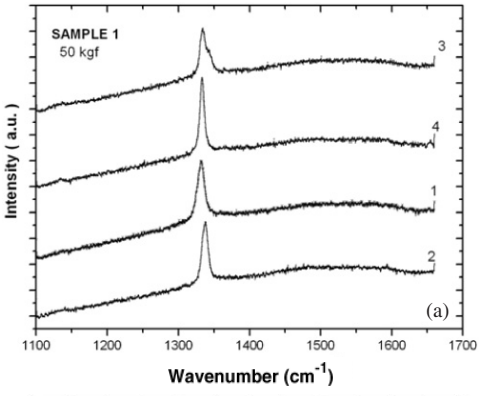

Figure 6. Raman spectra for samples (a) 1, (b) 2 and (c) 3 where each Raman line represents points 1–13 (as shown in figure 3). It is important to note that a 490 N indentation load was imposed on the samples, after which the samples were analysed using micro-Raman spectroscopy.

representing positions 6 and 9 was observed, which suggests that the stress levels in this region and its vicinity are high. It is most likely that the mechanical stress imposed on the coating during indentation loading exceeds the adhesion strength limit, and thus the coating fails and breaks off along and across the radial crack lines. A similar explanation could be valid in explaining the peak splitting in sample 1 at position 3.

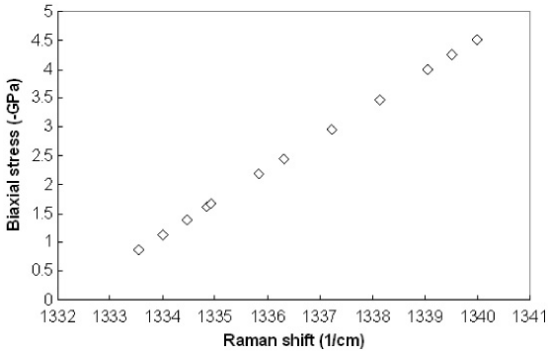

Figure 7. A graphical representation of the relationship between biaxial stress values and Raman peak shifts. The points used to plot the graph were obtained from tables 2 and 3.

The indentation tests showed that sample 3 presented a different response to the indentations imposed on its surface at both 294 and 490 N loads. The Raman spectra in figure 6(c) shows that the peak representing point 11 splits. This is consistent with our findings so far in relation to the monitoring of stress levels in or around the deformed zone. The Raman peak position at point 12 on sample 3 was 1334.46 cm^{-1}, which suggests that, in comparison, the adhesion strength at this point within the deformed zone is better than in samples 1 and 2.

As a summary, the Raman spectroscopy results suggest that in and around the impression mark, where deformation occurs by indentation loading, the increase in biaxial stresses resulted in the improvement of adhesion strength. This significant finding seems to be in contradiction with the common assumption that a higher residual stress leads to poor coating adhesion. However, these results are in agreement with our earlier investigations on assessing the adhesion strength of diamond coatings deposited using the conventional CVD growth mode on copper [43], chromium and titanium substrates [44]. Figure 7 shows the graph relating Raman shift to biaxial stresses. The calculated values for biaxial stress, as shown in tables 2 and 3, were used to construct the graph. It can be seen that the biaxial stress increases linearly with shift in the Raman peak position away from 1332 cm^{-1} wavenumbers. From our findings in the indentation tests and the micro-Raman spectroscopy analysis, we can state, with some degree of certainty, that the TMCVD process produces comparatively adherent diamond coatings onto micro-grain WC–Co substrates. We found in our earlier investigation [39] that the TMCVD process was effective in considerably reducing the time required to produce the first diamond layer, consisting of nano-sized diamond grains, on micro-grain WC–Co substrates. The rapid formation of the diamond layer during diamond deposition using TMCVD and the production of nano-grains can be held responsible for the improvements in the coating adhesion of the resultant films deposited onto WC–Co substrates by strengthening the substrate/film interface bond.

It should be noted that the diamond Raman shift also depends on the film thickness and the substrate material used to deposit the diamond coatings [45, 46]. In our case, the film thickness of each of the film coatings in samples 1–3 was equal (approx. 1 μm). The quality of the as-deposited films in samples 1–3 was almost identical, as there were no graphitic, amorphous or non-diamond phases present in the Raman spectra. Furthermore, intrinsic stresses can play a critical role in governing the Raman shift. Intrinsic stresses can change during diamond CVD growth, which can contribute to Raman peak shifting. Therefore, comparing the coating adhesion using the principle of Raman peak shifting should ideally be performed with the same kind of substrates and similar films, as was the case in the investigation.

4. Conclusions

The following conclusions can be drawn from this study.

(i) From the 294 N load indentation tests; it is indicative that sample 3 displayed better adhesion, since the diamond coating in sample 3 did not undergo lateral cracking. Samples 1 and 2 displayed a structure of the deformed zone on the coating consisting of lateral cracks, which resembled a shining sun.

(ii) On bare, uncoated WC–Co substrates, lateral cracks on the substrate surface appear only after 490 N load indentations. This result proves that the lateral cracks appearing in samples 1 and 2 at 294 N load indentations were due to the weak adhesion strength at the film/substrate interface.

(iii) Indentations at 490 N load inflicted significant damage on samples 1 and 2, in particular on sample 2. This suggests that the adhesion strength of samples 1 and 2 is not sufficient to withstand the indentation loading without any significant damage. Lateral cracks began to appear on sample 3, which was prepared using the TMCVD process, at 490 N load indentations. However, it could be that first the substrate fails, i.e. lateral crack lines appear, and as a result damage is inflicted on the overlaying coating.

(iv) Micro-Raman spectroscopy was used to assist the biaxial stress calculations. The degree of shifting of the Raman diamond peak towards and away from the standard diamond characteristic peak position, centred at 1332 cm^{-1}, was used to determine the attachment or detachment of the film coatings to the WC–Co substrates. It was found that the splitting of the diamond peak in the Raman spectra signalled spots on the coating surface where delamination had occurred. Furthermore, a greater degree of biaxial stress in the film coatings was correlated to stronger adhesion between the film coating and the WC–Co substrate.

(v) A 625 N indentation load was sufficient to delaminate the film coating in sample 3. Therefore, this implies that the critical load required to delaminate the coating in sample 3 lies in the range 294–490 N.

The authors are currently studying the influence of CH_4 pulse duty cycles on the mechanical interlock at the film/substrate interface and further improving and understanding better the coating adhesion and its behaviour on different grades of WC–Co materials.

Acknowledgment

N Ali and E Titus are grateful to FCT (Portugal) for financial support.

References

[1] Field J E (ed) 1992 *Properties of Natural and Synthetic Diamond* (San Diego, CA: Academic) p 667
[2] Angus J C and Hayman C C 1988 *Science* **241** 913
[3] Spear K E 1989 *J. Am. Ceram. Soc.* **72** 171
[4] Yarbrough W A and Messier R 1990 *Science* **247** 688
[5] Nesladek M, Spinnewyn J, Asinari C, Lebout R and Lorent R 1993 *Diamond Relat. Mater.* **3** 98
[6] Ong T P and Chang R P H 1991 *Appl. Phys. Lett.* **58** 358
[7] Weiser P S, Prawer S, Hoffman A, Manory R R, Paterson P J K and Stuart S A 1992 *J. Appl. Phys.* **72** 4643
[8] Ashfold M N R, May P W, Rego C A and Everitt N M 1994 *Chem. Soc. Rev.* **23** 21
[9] Hartsell M L and Plano L S 1994 *J. Mater. Res.* **9** 921
[10] Fan Q H, Gracio J and Pereira E 1998 *J. Mater. Res.* **13** 2787
[11] Brookes K J A (ed) 1996 *World Directory and Handbook of Hardmetals and Hard Materials* 6th edn (International Carbide Data)

[12] Sein H, Ahmed W, Hassan I U, Ali N, Gracio J and Jackson M J 2002 *J. Mater. Sci.* **37** 5057–63
[13] Sein H, Ahmed W, Jackson M, Ali N and Gracio J 2003 *Surf. Coat. Technol.* **163/164** 196–202
[14] Rajab H, Ali N, Sein H and Ahmed W 2000 *Mater. World* **8** 17
[15] Sein H, Ahmed W, Rego C A, Jones A N, Amar M, Jackson M and Polini R 2003 *J. Phys.: Condens. Matter* **15** S2961
[16] Oles E J, Inspektor A and Bauer C E 1996 *Diamond Relat. Mater.* **5** 617
[17] Haubner R and Lux A K B 2002 *Diamond Relat. Mater.* **11** 555–561
[18] Oakes J, Pan X X, Haubner R and Lux B 1991 *Surf. Coat. Technol.* **47** 600
[19] Mehlmann A K, Fayer A, Dirnfeld S, Avigal Y, Porath R and Kochman A 1993 *Diamond Relat. Mater.* **2** 317
[20] Singh R K, Gilbert D R, Fitz-Gerald J, Harkness S and Lee D G 1996 *Science* **272** 396
[21] Zang B and Zhou L 1997 *Thin Solid Films* **307** 21
[22] Sun F H, Zhang Z M, Chen M and Shen H S 2002 *J. Mater. Process. Technol.* **129** 435
[23] Sun F H, Zhang Z M, Chen M and Shen H S 2003 *Diamond Relat. Mater.* **12** 711
[24] Park J-K, Lee W-S and Baik Y-J 2003 *Surf. Coat. Technol.* **171** 1
[25] Tiejun L, Qihong L, Jingxing D, Yunrong W, Jun Z, Jingru L, Zhiming Z and Fanhong S 2002 *Appl. Surf. Sci.* 102
[26] Zhang Z M, Shen H S, Sun F H, He X C and Wan Y Z 2001 *Diamond Relat. Mater.* **10** 33
[27] Zhnag Z M, He X C, Shen H S, Sun F H, Chen M and Wan Y Z 2000 *Diamond Relat. Mater.* **9** 1749
[28] Neto M A, Fan Q H and Pereira E 2001 *Diamond Relat. Mater.* **10** 316–21
[29] Oakes J, Pan X X, Haubner R and Lux B 1991 *Surf. Coat. Technol.* **47** 600
[30] Haubner R, Kopf A and Lux B 2002 *Diamond Relat. Mater.* **11** 555
[31] Endler I, Leonhardt A, Scheibe H-J and Born R 1996 *Diamond Relat. Mater.* **5** 299–303
[32] Ali N, Ahmed W and Hassan I U 1998 *Mater. World* **6** 348
[33] Fan Q H, Ali N, Ahmed W, Kousar Y and Gracio J 2002 *J. Mater. Res.* **17** 1563
[34] Gusev M B, Babaev V G, Khvostov V V, Lopez Ludena G M, Brebadze A Yu, Koyashin I Y and Alexenko A E 1997 *Diamond Relat. Mater.* **6** 89–94
[35] Bull S J and Rickerby D S 1991 *Advanced Surface Coatings: a Handbook of Surface Engineering* ed D S Rickerby and A Matthews (New York: Chapman and Hall) p 315
[36] Ali N, Neto V F and Gracio J 2003 *J. Mater. Res.* **18** 298
[37] Wagner J, Wild C and Koidl P 1991 *Appl. Phys. Lett* **59** 779
[38] Collins A T 1996 *Enrico Fermi Summer Course on the Physics of Diamond (Italy, July–August 1996)* International School of Physics
[39] Ali N, Cabral G, Lopes A B and Grácio J 2004 *Diamond Relat. Mater.* **13** 498
[40] Knight D S and White W B 1989 *J. Mater. Res.* **4** 385
[41] Ager J W and Drory M D 1993 *Phys. Rev.* B **48** 2601
[42] Ralchenko V G, Smolin A A, Pereverzev V G, Obraztsova E D, Korotoushenko K G, Konov V I, Lakhotkin Yu V and Loubnin E N 1995 *Diamond Relat. Mater.* **4** 754
[43] Fan Q H, Gracio J and Pereira E 1999 *J. Appl. Phys.* **86** 5509
[44] Ali N, Ahmed W, Fan Q H and Rego C A 2000 *Diamond Relat. Mater.* **9** 1464
[45] Fan Q H, Fernandes A, Pereira E and Grácio J 1998 *J. Appl. Phys.* **84** 3155
[46] Fan Q H, Gracio J and Pereira E 1999 *Diamond Relat. Mater.* **8** 645